Prospects for detecting and localizing short-duration transient gravitational waves from glitching neutron stars without electromagnetic counterparts

Dixeena Lopez, Shubhanshu Tiwari, Marco Drago, David Keitel, Claudia Lazzaro, and Giovanni Andrea Prodi

Phys. Rev. D **106**, 103037 — Published 28 November 2022

DOI: 10.1103/PhysRevD.106.103037

Prospects for detecting and localizing short-duration transient gravitational waves from glitching neutron stars without electromagnetic counterparts

Dixeena Lopez,[1] Shubhanshu Tiwari,[1] Marco Drago,[2,3] David Keitel,[4] Claudia Lazzaro,[5,6] and Giovanni Andrea Prodi[7]

[1] *Physik-Institut, University of Zurich, Winterthurerstrasse 190, 8057 Zurich, Switzerland*
[2] *Dipartimento di Fisica, Università di Roma "La Sapienza", Piazzale Aldo Moro 2, I-00185 Roma, Italy*
[3] *INFN, Sezione di Roma, Piazzale Aldo Moro 2, I-00185 Roma, Italy*
[4] *Departament de Física, Universitat de les Illes Balears, IAC3–IEEC, Crta. Valldemossa km 7.5, E-07122 Palma, Spain*
[5] *Università degli Studi di Padova*
[6] *INFN sezione di Padova*
[7] *University of Trento, Physics Department and INFN, Trento Institute for Fundamental Physics and Applications, via Sommarive 14, 38123 Povo, Trento, Italy*

Neutron stars are known to show accelerated spin-up of their rotational frequency called a glitch. Highly magnetized rotating neutron stars (pulsars) are frequently observed by radio telescopes (and in other frequencies), where the glitch is observed as irregular arrival times of pulses which are otherwise very regular. A glitch in an isolated neutron star can excite the fundamental (f)-mode oscillations which can lead to gravitational wave generation. This gravitational wave signal associated with stellar fluid oscillations has a damping time of $10 - 200\,\mathrm{ms}$ and occurs at the frequency range between $2.2 - 2.8\,\mathrm{kHz}$ for the equation of state and mass range considered in this work, which is within the detectable range of the current generation of ground-based detectors. Electromagnetic observations of pulsars (and hence pulsar glitches) require the pulsar to be oriented so that the jet is pointed towards the detector, but this is not a requirement for gravitational wave emission which is more isotropic and not jet-like. Hence, gravitational wave observations have the potential to uncover nearby neutron stars where the jet is not pointed towards the earth. In this work, we study the prospects of finding glitching neutron stars using a generic all-sky search for short-duration gravitational wave transients. The analysis covers the high-frequency range from $1 - 4\,\mathrm{kHz}$ of LIGO–Virgo detectors for signals up to a few seconds. We set upper limits for the third observing run of the LIGO–Virgo detectors and present the prospects for upcoming observing runs of LIGO, Virgo, KAGRA, and LIGO India. We find the detectable glitch size will be around $10^{-5}\,\mathrm{Hz}$ for the fifth observing run for pulsars with spin frequency and distance comparable to the Vela pulsar. We also present the prospects of localizing the direction in the sky of these sources with gravitational waves alone, which can facilitate electromagnetic follow-up. We find that for the five detector configuration, the localization capability for a glitch size of $10^{-5}\,\mathrm{Hz}$ is around 132 square degrees at 1σ confidence for 50% of events with distance and spin frequency as that of Vela.

I. INTRODUCTION

Neutron stars (NSs) are one of the most promising and versatile sources of gravitational waves (GWs) [1], including both isolated NSs and those in binary systems with other compact objects. Several searches use varied methods for different scenarios depending on the nature of the targeted GW signals. Advanced LIGO [2] and Advanced Virgo [3] have detected GW signals from compact binary coalescences (CBCs), including binary neutron star coalescences (BNSs) and neutron star–black hole coalescences (NSBHs) [4–6]. Non-radial oscillation modes, magnetic or thermal mountains for both isolated NSs and those in binaries, as well as accretion in binary systems are among the sources for continuous GWs [7]. Isolated NSs are also an interesting astrophysical source for transient GWs in the detectable range of current generation GW detectors. For example, searches have been conducted for magnetars that can be strong emitters of transient GWs and short bursts of γ-rays [8, 9], but no detection has been made yet.

In this paper, we will focus on transient GWs from glitching pulsars. Rotating isolated NSs, including pulsars, generally show a decrease in their spin frequency over time. However, some exhibit a sudden jump in their rotation frequency known as glitches [10]. So far, at least 740 glitches from 225 known pulsars have been reported with glitch sizes of $\Delta\nu_s \approx 10^{-9}$–$10^{-4}\,\mathrm{Hz}$ [11–16].

Glitches in isolated neutron stars can excite acoustic and inertial stellar oscillations which in turn generate GWs lasting $\lesssim 0.2\,\mathrm{s}$ at frequencies from 1–3 kHz depending on the models and source parameters. f-mode oscillations are among these potential causes of GW emission [17, 18]. Recently, a scenario for GWs from f-modes in smaller glitch candidate events was also studied [19]. Historically, a first targeted search for short transient GWs associated with a glitch was conducted for a Vela pulsar glitch in August 2006, finding no evidence of GWs [20]. More recently, a generic all-sky search for GW transients during the third observing run [21] was also interpreted under the glitch scenario, providing a limit on minimum detectable glitch size around $10^{-4}\,\mathrm{Hz}$ for an optimally oriented source and with Vela reference parameters. During the second observing run (O2) of Advanced LIGO and

Advanced Virgo (November 2016 - August 2017), four pulsar glitches were observed in radio telescopes based on [14]. Considering the whole glitch energy transformed as GW by the $f-$mode oscillation of NS, only the peak amplitude from the Vela glitch detected by the radio telescope on 2016 December 12 is above the power spectral density (PSD) of LIGO and Virgo detector during the O2 run [22, 23]. During the glitch in Vela, only LIGO Hanford was online out of three GW detectors, making GW counterpart detection unreliable [24]. In addition, searches for longer-duration quasi-monochromatic transient GWs correlated to pulsar glitches during the second and third observing runs [25–27] also put upper limits on GW strain under that scenario. Moreover, a recent study about the prospects for observing longer-duration GW signals with current and future ground-based detectors is given in [16]. However, in this paper we focus on shorter signals from f-modes.

In general, the population of isolated NSs observed by electromagnetic (EM) observatories is a small fraction of the actual NS population in our galaxy. Hence, all-sky GW searches have the potential to find previously undiscovered NSs. Follow-up searches of GW detections by EM observation, e.g. in the X-ray and radio bands, could then help in constraining NS properties. The sky localization information from the GW search is crucial to provide an opportunity for a targeted follow-up by EM telescopes.

This paper presents the all-sky search results for short-duration transient GWs from NS glitches during the third LIGO–Virgo observing run for arbitrarily oriented sources. We provide the prospects for future runs of the current generation of GW detectors regarding the glitch size one can probe. The future observing runs are expected to include KAGRA [28], LIGO India [29], and further upgrades of Advanced LIGO and Advanced Virgo. We also present the prospects for the sky localization of these sources for the upcoming observing runs.

The paper is organized as follows. Section II describes the signal model. Section III discusses the search for short transient GW signals from glitching NSs. Section IV discusses the prospects of observing and localizing these GW signals for future ground-based detector searches. Section V discusses the results.

II. SIGNAL MODEL

Two main mechanisms are considered to be responsible for pulsar glitches: starquakes and superfluid–crust interactions [20, 30–33]. The energy generated during the excitation of oscillation modes by the starquakes or superfluid–crust interactions is given as [18, 20, 30, 34],

$$\Delta E_{\rm glitch} \approx 4\pi^2 I \nu_{\rm s} \Delta\nu_{\rm s}\,, \tag{1}$$

where $I \sim 10^{38}\,{\rm kg\ m^2}$ is the stellar moment of inertia, $\nu_{\rm s}$ is the spin frequency and $\Delta\nu_{\rm s}$ is the increase in spin frequency [20]. An order of magnitude estimate can be obtained by comparing with fiducial values of the frequency and its change during the glitch. The energy can be expressed as [18, 20],

$$\Delta E_{\rm glitch} \approx 3.95\times10^{40}{\rm erg}\left(\frac{\nu_{\rm s}}{10\,{\rm Hz}}\right)\left(\frac{\Delta\nu_{\rm s}}{10^{-7}\,{\rm Hz}}\right). \tag{2}$$

A possible consequence of NS glitches is the excitation of one or more oscillations in the NS. This leads to the excitation of different families of pulsation modes like pressure p-modes (the fundamental of which is known as the f-mode) and the gravity g-modes corresponding to the energy of the glitch [18, 35–37]. In this work, we are interested in the f-modes, which are the dominant mode in producing transient GWs from NS glitches [38–40]. For a perfectly spherical NS (non-rotating, non-magnetic), the damping time and mode frequency are degenerate for each mode. Moreover, we consider only the dominant quadrupolar emission ($l = 2$) here as higher-order modes ($l > 2$) will be sub-dominant [41, 42] and also will occur at a higher frequency where the detectors lose sensitivity [43]. Hence, GWs associated with the excitation of pulsation modes (f-modes) are short-lived signals, which can be expressed in the time domain as [18, 44],

$$h(t) = h_0 e^{-t/\tau_{\rm gw}}\sin(2\pi\nu_{\rm gw}t)\,. \tag{3}$$

Here, h_0 is the initial amplitude of the signal. $\nu_{\rm gw}$ and $\tau_{\rm gw}$ are the frequency and characteristic damping time of the signal, respectively.

The initial amplitude is related to the total GW energy emitted by a source at a distance d [18, 20, 45]:

$$h_0 = \frac{1}{\pi d\nu_{\rm gw}}\left(\frac{5G}{c^3}\frac{E_{\rm gw}}{\tau_{\rm gw}}\right)^{1/2}. \tag{4}$$

Therefore the peak GW amplitude of the $f-$mode ringdown signal, assuming the total energy generated by the excitation of the dominant mode is emitted as GWs ($E_{\rm gw} \approx E_{\rm glitch}$) is given as (eq.5 of [18]),

$$h_0 = 7.21\times10^{-24}\left(\frac{1\,{\rm kpc}}{d}\right)\left(\frac{\nu_{\rm s}}{10\,{\rm Hz}}\right)^{1/2} \left(\frac{\Delta\nu_{\rm s}}{10^{-7}\,{\rm Hz}}\right)^{1/2}\left(\frac{1\,{\rm kHz}}{\nu_{\rm gw}}\right)\left(\frac{0.1\,{\rm s}}{\tau_{\rm gw}}\right)^{1/2}. \tag{5}$$

Quasinormal modes are classified according to the restoring force, which brings the perturbed element of the fluid back to the equilibrium position. We consider the non-rotating limit where only GWs from f-mode oscillations are well inside the sensitive bandwidth of ground-based GW detectors [17]. Empirical relations for frequencies and damping times as functions of the mean mass density and compactness for various equations of state (EoS) are given as [46],

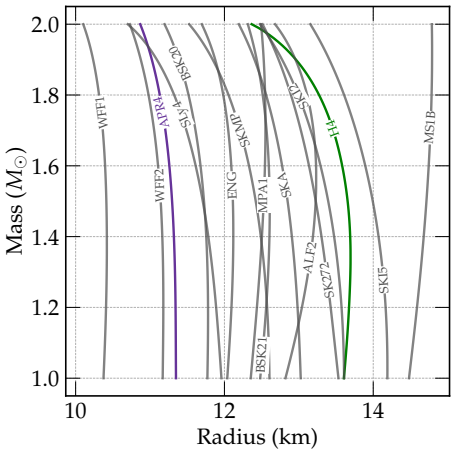

FIG. 1. The mass–radius curves for a sample of EoSs, over a mass range of $1-2\,M_\odot$. We choose the APR4 (purple) and H4 (green) EoS for this study, representing more and less compact NSs respectively. Produced using LALSimulation [47, 48].

$$\nu_{\rm gw}[{\rm kHz}] = 1.562 + 1.151\left(\frac{\bar{M}}{\bar{R}^3}\right)^{1/2} \tag{6}$$

and

$$\frac{1}{\tau_{\rm gw}[\ {\rm s}]} = \frac{\bar{M}^3}{\bar{R}^4}\left[78.55 - 46.71\left(\frac{\bar{M}}{\bar{R}}\right)\right], \tag{7}$$

where

$$\bar{M} = \frac{M}{1.4\,M_\odot} \quad \text{and} \quad \bar{R} = \frac{R}{10\,{\rm km}}. \tag{8}$$

Here we consider the Cowling approximation [35, 49], where the perturbations of the metric are neglected and only fluid perturbations are taken into account [46]. Each nuclear-matter EoS generates a unique relation between the mass and radius of NSs [50]. We need that mass–radius relation to use the empirical relations given above for the frequency and damping time. But the EoS of NSs is currently not precisely known. However, there are constraints on the EoS from EM and GW observations [51]. The mass–radius relation for non-rotating NS models with various EoS [48, 52] for masses between $1-2\,M_\odot$ are shown in Fig. 1. In this work, we choose two different EoS namely APR4 [53] and H4 [54], which are considered as representatives for the classes of soft (more compact) and hard (less compact) models respectively.

For the different cases of EoSs from Fig. 1, we compute the relation given in Eqn. 6 and Eqn. 7 to obtain the dependency of GW signal properties (frequency and damping time) as a function of NS mass as shown in Fig. 2. For the typical masses of NSs between $1-2\,M_\odot$, we obtain corresponding f-mode frequencies between $2.2-2.8\,$kHz [55]. As the mass of the NS increases, the f-mode frequency increases. Also, we can infer that for the softer

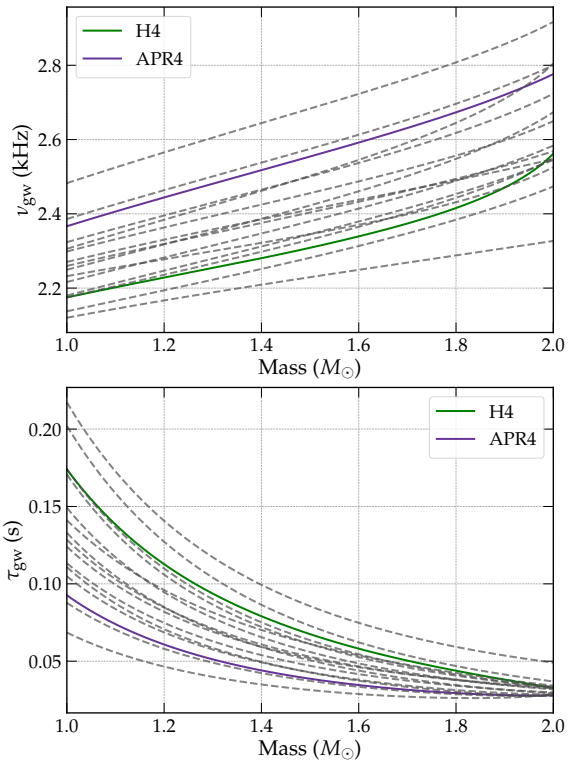

FIG. 2. GW frequency (top panel) and damping time (bottom panel) as a function of NS mass according to Eqn. 6 and Eqn. 7 for the cases of EoSs refereed in Fig. 1. We choose two EoSs representing soft (APR4) and hard (H4) in this work. The grey dotted lines represent the other EoSs from Fig. 1.

EoS the frequency is systematically higher than that for the harder EoS. One can speculate that a confident detection of GWs from an NS glitch with a sufficiently accurate frequency estimation will contain information about the EoS, which is degenerate with NS mass but not in the entirety of the parameter space. In Fig. 2, we also show the distribution of the damping time $\tau_{\rm gw}$. The damping times decrease as the mass of the NS increases and it should be noted that for the softer EoS the damping time drops off faster than for the harder EoS.

A comparison study for the GW frequency from $f-$mode oscillation as a function of mean mass density from previous literature is given in Appendix A. The Cowling approximation used in Eqn. 6 results in an overestimate of the frequency by about 30%. However, using it in the following analysis can be considered a conservative choice as GW detector sensitivities in the kHz regime fall off as the frequency increases.

III. ANALYSIS OVERVIEW

A. Search method and data

We consider an all-sky search for generic short-duration GW transients using the coherent WaveBurst (cWB) pipeline [56]. cWB is a morphology-independent algorithm for the detection and reconstruction of GW transients. It is based on maximum likelihood-ratio statistics applied to excess power above the detector noise in the multi-resolution time–frequency (T–F) representation of GW strain data [56–58]. We use the same version of cWB as was used for the LIGO–Virgo–KAGRA collaboration's third observing run (O3) high-frequency search for generic transients [21], with the same settings.

As discussed in Section II and also in [17, 46], GWs from f-mode oscillations in glitching pulsars will occur in the high-frequency range ($2.2 - 2.8\,\mathrm{kHz}$) of ground-based detectors. Therefore, we restrict our analysis to the frequency range of $1 - 4\,\mathrm{kHz}$. We have analyzed the publicly available O3 data, which extended from April 1, 2019 to March 1, 2020 [21, 59]. For these O3 results, we consider only the Hanford–Livingston (HL) network since Virgo has a significant sensitivity imbalance for frequencies higher than 1 kHz (almost a factor 5). For the near future prospects of detecting GWs from NS glitches in the fourth (O4) and fifth (O5) observing runs, we have generated Gaussian noise based on the expected spectral sensitivities for the three-detector network with both LIGOs and Virgo [60]. Fig. 3 shows the sensitivities of the detectors in terms of measured noise amplitude spectral densities from O3 and the expected curves for O4 and O5 [61].

Background generation

The background is generated by time-shifting the detector's data with respect to the reference detector. For O3, we have used the data from the two LIGO detectors (Livingston and Hanford) and produced over 500 years of time-shifted background with approximately 200 days of available coincident observing time. For O4 and O5, we have simulated 16.85 days of data for the LIGO and Virgo detectors by assuming Gaussian noise which follows the PSD for the corresponding detector and observing run. From this data, we have produced 23 years of background by a time-shifting of LIGO Hanford and Virgo by keeping LIGO Livingston as a reference. For O3, the most significant trigger had a False-Alarm Rate of about 1 event in 0.3 years which is well within the expected background rate (assuming the detectors' glitches follow a Poisson distribution, the significance is 0.5 sigma). The central frequency of this trigger was 2.1 kHz [21].

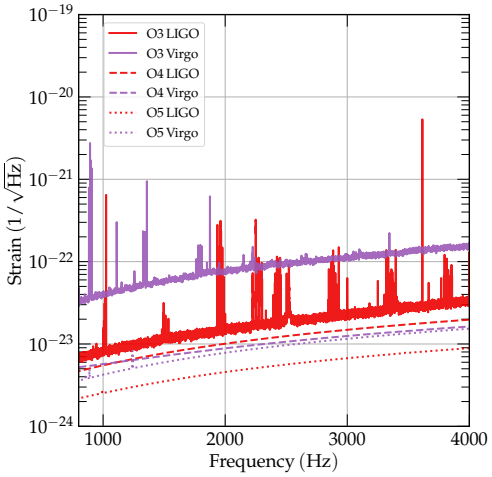

FIG. 3. Noise amplitude spectral densities of the LIGO Livingston and Virgo detectors for O3 (measured) as well as predictions for O4 and O5 in the high-frequency range.

B. Injection set

To compute the detection sensitivity of this high-frequency all-sky search setup with a given detector configuration, we perform an injection study of adding simulated damped sinusoid waveforms to the detector data for O3, O4 and O5 runs.

In this work, we have used a different injection set in terms of the extrinsic parameters of the signals as compared to the results presented in [21]. In [21], the distribution of the simulated sources in the sky was uniform. Here we have used a distribution in sky directions that is uniform over the galactic disk based on the Miyamoto-Nagai Galactic Disk Model [62, 63]. Also, in [21] the inclination angle of all sources was chosen as face-on (optimally oriented), whereas here we sample uniformly over the full range of inclination angles. The injections are distributed in terms of root-mean-squared amplitude, $h_{\mathrm{rss}} = \sqrt{\int_{-\infty}^{\infty} \left(h_+^2(t) + h_\times^2(t)\right) \mathrm{d}t}$ as in [21] with injected h_{rss} value givens by $(\sqrt{3})^{\mathrm{N}} 5 \times 10^{-23}$ Hz$^{-1/2}$, for N ranges from 0 to 8.

As discussed in section II, the intrinsic parameters of the damped sinusoids (frequency and damping time) can be related to the source parameters (mass and EoS of the NS). The mass of the NS is considered from $1-2\,M_\odot$ with a bin size of $0.25\,M_\odot$. The injection sets are built for each mass bin of the two EoSs considered for this work, which leads to eight injection sets. Fig. 4 shows the distribution of the frequency and damping time of the waveform in the injection set. Each of the eight injection sets considered here is populated with more than 100,000 injections for O3 and 40,000 injections for O4 and O5, providing a precise measurement of the detection efficiency.

The amplitude of the incoming signal is a function of distance to the source, spin frequency of the NS and glitch size. To interpret the results one can fix any two of the

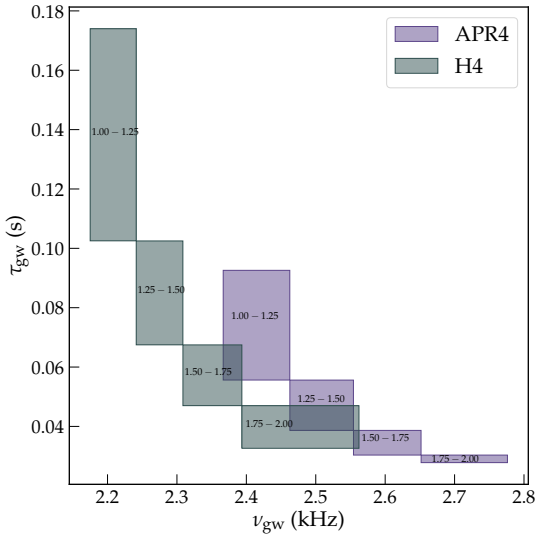

FIG. 4. Distribution of intrinsic parameters, (GW frequency and damping time) of injected damped sinusoid waveforms for the four mass bins of the EoS, APR4 and H4. The width and height of each box indicate the spread in frequency and damping time for each injection set.

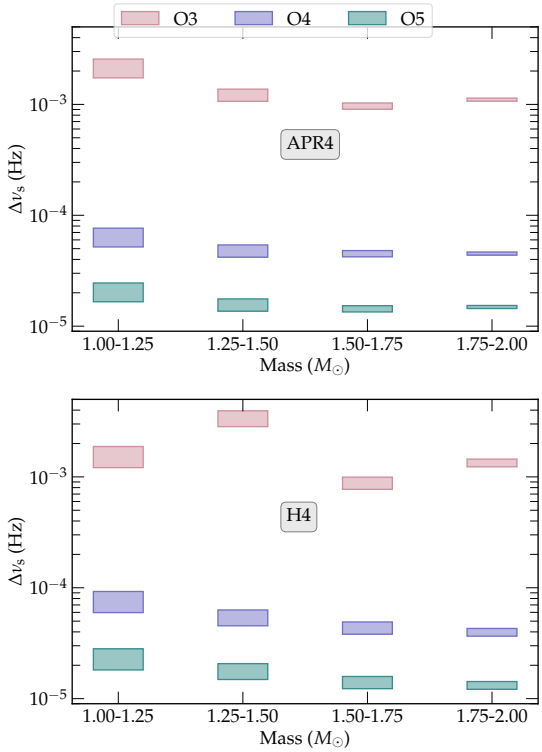

FIG. 5. Sensitivity of the high-frequency all-sky transient search during the O3 run in terms of detectable NS glitch sizes. The corresponding expected sensitivities for O4 and O5 using their predicted noise curves are also shown. Signals are simulated using the spin frequency and distance of the Vela pulsar, other source parameters are drawn from distributions as described in the text with NS models following two different EoS (APR4 and H4). The sensitivities are shown as separated into four mass bins between $1-2\,M_\odot$. The variation in detectable glitch size within each mass bin is indicated by the vertical height of the box for each bin. The glitch size is computed from the minimum $h_{\rm rss}$ needed for 50% detection efficiency at iFAR$\geq$ 10 years. We consider the HL network for O3 results and the HLV network for the O4 and O5 runs.

parameters listed above. We fix the distance of the source to that of the Vela pulsar at 287 pc [64]. (For clarity, we underline that we do not fix the sky direction to that of Vela, just the distance.) We also fix the spin frequency of the NS to approximately that of Vela ($\nu_{\rm s} = 11.2$ Hz) [65] and hence we discuss the results in terms of glitch size.

C. Sensitivity to GW signals during pulsar glitches

The sensitivity is determined using the value of the quantity $h_{\rm rss}$ needed to achieve 50% detection efficiency for each mass bin and EoS at an inverse False-Alarm Rate (iFAR) larger than 10 years. We keep the parameters distance and spin frequency fixed to those of the Vela pulsar and interpret the result in terms of glitch size $\Delta\nu_{\rm s}$ using Eqn. 5. Here the peak amplitude, h_0 is computed from $h_{\rm rss}$ numerically. Fig. 5 reports the limit on detectable glitch size as a function of mass and EoS for the O3 run, as well as projected detectable glitch sizes for the future O4 and O5 sensitivities.

In [21], the detectable glitch size for optimally oriented sources (uniformly distributed in all sky directions) was greater than 10^{-4} Hz. Under the uniform galactic source distribution, for O3 we find that we would have needed a glitch size larger than $\approx 10^{-3}$ Hz to confidently detect 50% of events. This difference arises mainly from loosening the condition of optimal orientation. For O4 we see around an order of magnitude improvement for the detectable glitch size across the mass bins for both cases of EoS as compared to O3. For O5 this is around two orders of magnitude improvement in detectable glitch size. These improvements are attributed both to improvements in each detector but also the inclusion of Virgo, which allows injections to be recovered from a wider portion of the sky.

The assumption of Gaussian noise (which we make for future observing runs) is not too far from reality for the high-frequency range of the detectors. However, non-stationary lines [66, 67] are present in real data. These lines lead to an anomalously inadequate sensitivity visible in the results (Fig. 5) for the H4 EoS mass bin $1.25-1.5\,M_\odot$. Following up on this, we found that this reduced sensitivity correlates with a population of lines occurring between $2.2-2.3$ kHz, which reduces the sensitivity of the detectors for signals falling in this frequency range, leading to higher glitch sizes needed for detections in this mass bin.

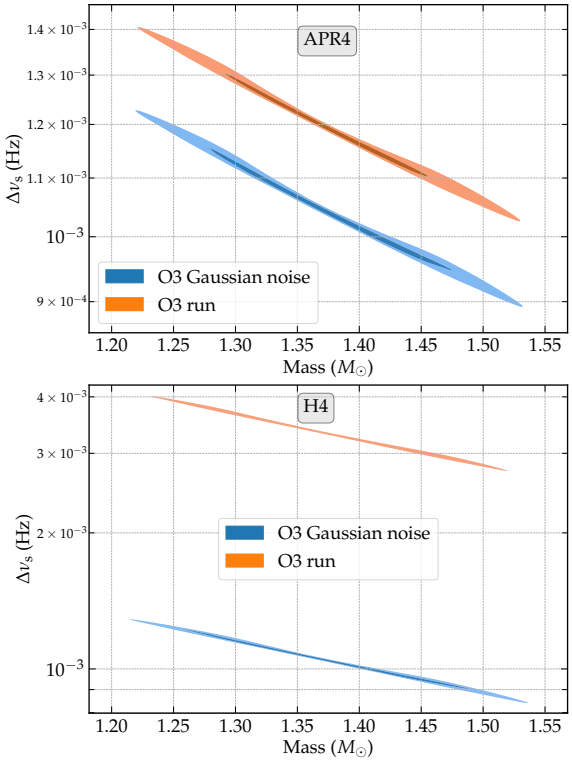

FIG. 6. Difference in detectable glitch sizes obtained from the real O3 data compared with simulated Gaussian noise at O3 detector sensitivity. The injected waveforms are for APR4 and H4 EoS with a mass range between $1.25-1.50\,M_\odot$. It can be seen that the non-stationary lines at $2.2-2.3$ kHz hinder the detectability of H4 EoS signals in this mass range, whereas for APR4 signals which do not fall near the non-stationary lines, detectability is similar in real data and Gaussian noise.

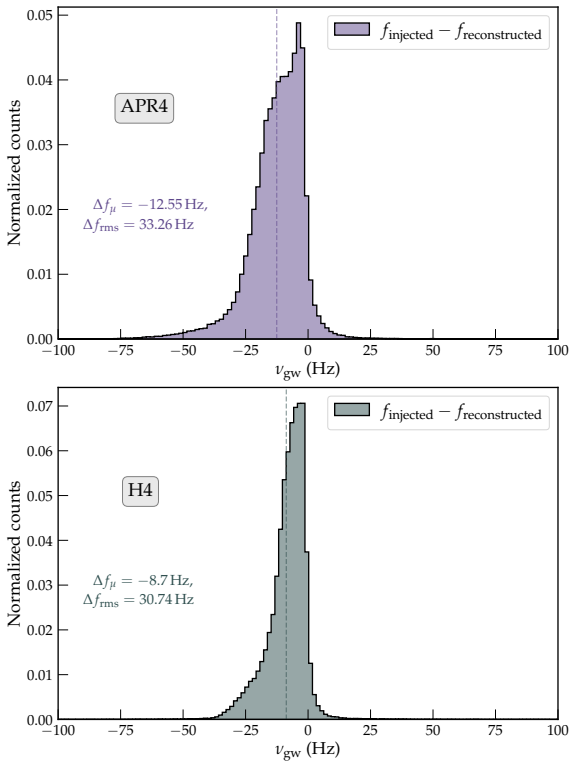

FIG. 7. Difference between the injected and reconstructed central frequencies (Δf) are plotted for O3 data for the mass bin $1.25-1.50\,M_\odot$ and the two EoS considered. We show the mean Δf_μ and rms $\Delta f_{\rm rms}$ of the distribution. Given the frequencies are over 2 kHz the mean and rms are less than 1%.

We conducted an additional study to quantify this hypothesis that indeed the noise happening between 2.2–2.3 kHz during the O3 run causes this reduction in sensitivity. For this, we generated simulated data with Gaussian noise based on O3 noise spectral density [61] and computed the detectable glitch size at iFAR higher than 10 years. We found a factor of 3.35 improvement with Gaussian noise as compared to real O3 noise as shown in Fig. 6. If we take this into account, this outlier mass bin in H4 EoS with worse sensitivity can be explained. This also outlines the fact that the main challenge for the practical implementation of this analysis in future observing runs will be the mitigation of wandering lines in the high-frequency part of the parameter space.

D. Reconstruction of signal's frequency

In this section, we briefly report the capability of our search algorithm to reconstruct the injected signal's central frequency. The central frequency of both injected and reconstructed signal is defined as the energy averaged frequency of all the pixels representing the signal. The robust reconstruction of the frequency is necessary for the identification of the trigger as a possible candidate coming from glitching NS. This can allow for further follow-up with dedicated parameter estimation and search for EM counterparts.

The reconstruction of the signal's central frequency is shown in Fig. 7. The example shown here is for the O3 data for a mass bin of $1.25-1.50\,M_\odot$ for the two EoS considered in this paper. For all the other injection sets the results are similar. We show the difference between the injected and recovered frequencies and find that the mean is reconstructed with slightly higher frequencies with a bias of less than 0.5% and a root-mean-square (rms) of 1%.

IV. PROSPECTS FOR LOCALIZING GLITCHING NS FROM GW DETECTION

Since we are looking to unveil a population of nearby NSs which may not yet have been observed in the EM spectrum, sky localization of the sources of GW detections will play a key role in enabling the follow-up of these events by various ground and space-based telescopes. Even if the GW signal is associated in time with

an EM transient, we would still need sky direction information to unambiguously associate the events. In this section, we provide a study on the sky localization capabilities of different networks of GW detectors.

Sky localization with a network of GW detectors mainly relies upon the time delay measurement between various detectors. Given a pair of detectors, the time of arrival and the amplitude will localize the signal to a ring in the sky [68, 69]. If we have three detectors and hence two pairs, we can localize a source to a much smaller region around the intersection of the two circles in the sky corresponding to each pair of detectors. Longer baselines between detectors and a higher number of detectors lead to better localization [70].

In the case of cWB, the likelihood is computed and is maximized over sky directions, which is very sensitive to the time delays, antenna pattern response and polarization of incoming GWs. The reconstructed sky direction statistic is a function of the likelihood. Further discussion about the properties of the sky statistics of cWB can be found in Section 3 of [57].

Here we study the prospects for localizing GW transients from a NS glitch considering the example of APR4 EoS for masses between $1.25 - 1.5\,M_\odot$ and using simulated Gaussian noise for the O5 run. Although we have considered only one injection set for this study, for the other injection sets the results are not expected to change significantly. We inject the NS glitch waveforms in the simulated data corresponding to the spin frequency and distance of the Vela pulsar with five glitch size values spaced between 10^{-6} Hz and 10^{-3} Hz. For each considered glitch size, the sources are uniformly distributed in sky direction and source orientation, the same as in [21] to get the maximum efficiency. The metric we use here to determine typical sky localization performance is the sky error region at 1σ credible interval for 50% of the detected events[71]. We consider the following present and future detectors: LIGO-Hanford (H), LIGO-Livingston (L), Virgo (V), KAGRA (K), and LIGO-India (I), combining them in three different networks: LHV, LHVK, LHVIK. In Fig. 8 we show the cumulative histogram for the LHVIK network for glitch size 10^{-5} Hz as a function of the sky error region. We can see that only 10% of the detected events are localized better than 2 deg^2, whereas 50% of the events are localized with the sky error region better than 132 deg^2. With the choice of the sky error region for 50% of the events, we explore various network configurations and glitch sizes in Fig. 9.

As expected, a drastic improvement can be seen as the number of detectors in the network increases and also an improvement as the glitch size grows (since the signal-to-noise ratio grows with it). For a scenario discussed before of 10^{-5} Hz glitch size with the five detector network, we get the sky localization region of around 132 square degrees at 1σ uncertainty for 50% of events, which might be too large for many EM telescopes to efficiently follow up the full sky area, but there can be a few cases where the sky localization can be as good as a few deg^2. Compared with CBC localization areas in O1–O3 [4–6], this level of localization can still provide an opportunity to potentially find an EM counterpart to a transient burst GW detection from a glitching pulsar.

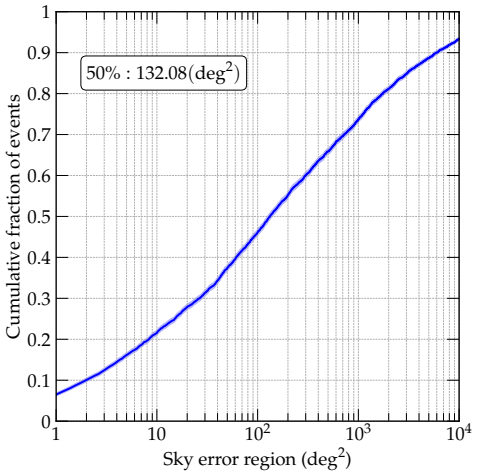

FIG. 8. Sky error region at 1σ credible interval (SER) for LHVIK network with O5 sensitivity. The blue curve shows the localization area for a cumulative fraction of events with the 1σ deviation shown in the shaded region. The analysis is illustrated for the injection set with APR4 EoS and mass range from $1.25 - 1.5\,M_\odot$ at injected $\Delta\nu_s$ of 1.849×10^{-5} Hz. 50% of injected events are recovered at 132.08 square degrees.

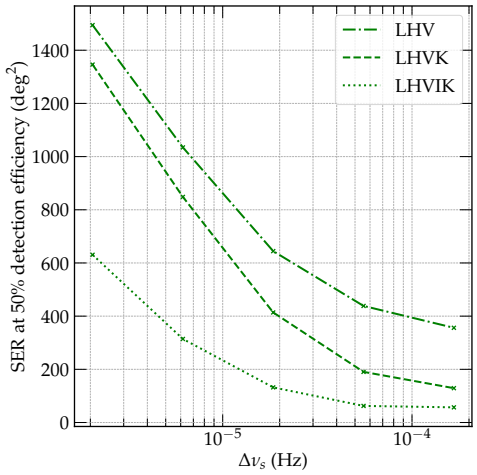

FIG. 9. Sky error region at 1σ credible interval (SER) as a function of NS glitch size assuming O5 sensitivity for the LHVIK, LHVK, and LHV networks. Specifically, this is the localization region size at 1σ confidence achieved by 50% of the events at a given glitch size. Here we used the APR4 EoS and NS masses between $1.25 - 1.5\,M_\odot$ to generate simulated signals.

V. DISCUSSIONS

In this work, we have updated the all-sky upper limits from the LIGO–Virgo O3 run for short-duration GW signals from f-modes triggered by glitches in NSs without electromagnetic counterparts by using more realistic distributions in the extrinsic parameters (i.e. sky direction and orientation of the source) of the simulated signals used for sensitivity estimation. We have also investigated how line artifacts in the O3 data affect sensitivity in certain frequency bands and hence source mass ranges, which sheds light on the practical challenges which we face for such high-frequency short-duration searches. Further, we give the prospects for the detection and localization of such short-duration GWs from NS glitches for the upcoming fourth (O4) and fifth (O5) observing runs of the current generation of ground-based detectors. By fixing the reference pulsar as Vela (in terms of distance and spin frequency), we found that the detectable glitch size will be around 10^{-4} Hz for O4 and 10^{-5} Hz for O5. Glitch sizes of 10^{-5} Hz have been observed by radio telescopes before [12, 65, 72]. Further, it has been shown that observed pulsar glitches form two different populations when it comes to glitch size [10, 73, 74]. These distributions are conventionally called *normal* or *Crab-like* for the smaller glitches and *Vela-like* for the larger (mean at around $10^{-4.4}$ Hz) glitches. Thus, for O4 and O5 there can be a more realistic chance to observe a nearby glitching pulsar if the glitch comes from the population of *Vela-like* glitches. We have also studied the localization capability of this type of GW searches, finding that with a five detector network during O5 for the detectable glitch sizes of 10^{-5} Hz the EM follow up can be challenging, as the sky error region for 50% events at 1σ is about 132 square degrees. However, this localization can still be useful for future wide-scope telescopes like CHIME, SKA, etc [75, 76]. It could also be sufficient to associate the GW event with the galactic disk.

The proposed third-generation GW observatories like Einstein Telescope [77], Cosmic Explorer [78], and NEMO [79] will provide much higher sensitivities at kHz ranges, ideal for observing GW signals from glitching pulsars. We leave it for future studies to quantify the sensitivity of third generation detectors, where the analysis methods and search configurations will need to be very different.

ACKNOWLEDGMENTS

We thank Leigh Smith for comments on an early version of this draft. The document has been given LIGO DCC number P2200190. DL acknowledges support from Swiss National Science Foundation (SNSF) grant number 200020-182047. ST is supported by Swiss National Science Foundation (SNSF) Ambizione Grant Number : PZ00P2-202204. MD acknowledges the support from the Amaldi Research Center funded by the MIUR program 'Dipartimento di Eccellenza' (CUP:B81I18001170001) and the Sapienza School for Advanced Studies (SSAS).

DK is supported by the Spanish Ministerio de Ciencia, Innovación y Universidades (ref. BEAGAL 18/00148) and cofinanced by the Universitat de les Illes Balears, and acknowledges support by European Union FEDER funds, the Spanish Ministerio de Ciencia e Innovación and Spanish Agencia Estatal de Investigación grants PID2019-106416GB-I00/MCIN/AEI/10.13039/501100011033, RED2018-102661-T, RED2018-102573-E, the European Union NextGenerationEU funds (PRTR-C17.I1); the Comunitat Autònoma de les Illes Balears through the Direcció General de Política Universitària i Recerca with funds from the Tourist Stay Tax Law ITS 2017-006 (PRD2018/24, PDR2020/11); the Conselleria de Fons Europeus, Universitat i Cultura del Govern de les Illes Balears; the Generalitat Valenciana (PROMETEO/2019/071), and EU COST Actions CA18108 and CA17137.

This research has made use of data obtained from the Gravitational Wave Open Science Center (https://www.gw-openscience.org), a service of LIGO Laboratory, the LIGO Scientific Collaboration and the Virgo Collaboration. The authors are grateful for computational resources provided by the LIGO Lab (CIT) and supported by National Science Foundation Grants PHY-0757058 and PHY-0823459. This material is based upon work supported by NSF's LIGO Laboratory which is a major facility fully funded by the National Science Foundation.

Appendix A: Comparison of f-mode frequencies

Here, we are looking for the frequency of a GW signal emitted by an f-mode oscillation during a glitch that is related to the mean density of the NS [17, 44, 46]. These relations are found from the solution of the non-radial perturbations equation of a non-rotating star in general relativity (GR) or using the Cowling approximation [80–87].

We compare our injected signal frequency with numerical relativity simulations solving the Einstein equations for dynamical spacetimes in full GR present in literature. The empirical fit for fundamental mode frequency ν in full GR with dynamical spacetime for a non-rotating star is given as,

$$\nu[\mathrm{kHz}] = k_l + \mu_l \left(\frac{\bar{M}}{\bar{R}^3}\right)^{1/2}. \tag{A1}$$

Table. I show the coefficients k_l and μ_l of Eqn. A1 for $l = 2$ given in different literature [17, 46, 87–92]. The corresponding GW frequency as a function of average density for the EoS, APR4 and H4 are shown in Fig. 10. It clearly shows the frequency is overestimated with the Cowling approximation in the non-rotating limit (Doneva 2013) [46].

Reference	k_2	μ_2
Doneva 2013	1.562	1.151
Andersson 1998	0.78	1.635
Benhar 2004	0.76	1.5
Chirenti 2015	0.332	2.005
Pradhan 2021	1.075	1.412
Das 2021	1.185	1.246
Mu 2022	-0.121	2.197
Pradhan 2022	0.535	1.648

TABLE I. Coefficients k_l and ν_l of Eqn. A1 ($l = 2$) for f-mode frequency from different literature.

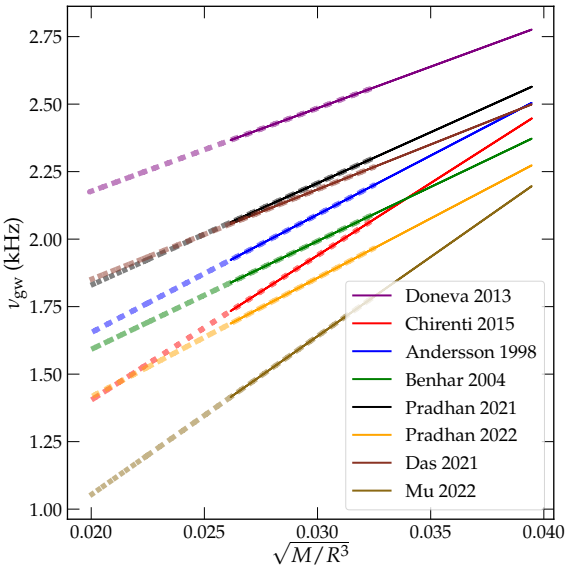

FIG. 10. Distribution of GW frequency as a function of NS mean density. Each curve shows the f-mode oscillation frequency derived using Eqn. A1 from the literature mentioned in table I. The solid (dotted) line shows the APR4 (H4) EoS for the NS mass ranges from $1 - 2\,M_\odot$.

[1] Kostas Glampedakis and Leonardo Gualtieri, "Gravitational waves from single neutron stars: An advanced detector era survey," in *The Physics and Astrophysics of Neutron Stars*, edited by Luciano Rezzolla *et al.* (Springer International Publishing, Cham, 2018) pp. 673–736.

[2] J Aasi *et al.*, "Advanced LIGO," Classical and Quantum Gravity **32**, 074001 (2015).

[3] F Acernese *et al.*, "Advanced virgo: a second-generation interferometric gravitational wave detector," Classical and Quantum Gravity **32**, 024001 (2014).

[4] B. P. Abbott *et al.* (LIGO Scientific Collaboration and Virgo Collaboration), "Gwtc-1: A gravitational-wave transient catalog of compact binary mergers observed by ligo and virgo during the first and second observing runs," Phys. Rev. X **9**, 031040 (2019).

[5] R. Abbott *et al.* (LIGO Scientific Collaboration and Virgo Collaboration), "Gwtc-2: Compact binary coalescences observed by ligo and virgo during the first half of the third observing run," Phys. Rev. X **11**, 021053 (2021).

[6] R. Abbott *et al.* (LIGO Scientific Collaboration, Virgo Collaboration and KAGRA Collaboration), "GWTC-3: Compact Binary Coalescences Observed by LIGO and Virgo During the Second Part of the Third Observing Run," arXiv:2111.03606.

[7] Keith Riles, "Searches for continuous-wave gravitational radiation," arXiv:2206.06447.

[8] B. P. Abbott *et al.* (LIGO Scientific Collaboration and Virgo Collaboration), "Search for Transient Gravitational-wave Signals Associated with Magnetar Bursts during Advanced LIGO's Second Observing Run," Astrophys. J. **874**, 163 (2019).

[9] R. Abbott *et al.* (LIGO Scientific Collaboration, Virgo Collaboration, and KAGRA Collaboration), "Search for Gravitational Waves Associated with Gamma-Ray Bursts Detected by Fermi and Swift during the LIGO–Virgo Run O3b," Astrophys. J. **928**, 186 (2022).

[10] J. R. Fuentes, C. M. Espinoza, A. Reisenegger, B. W. Stappers, B. Shaw, and A. G. Lyne, "The glitch activity of neutron stars," Astron. Astrophys. **608**, A131 (2017).

[11] Fuentes, J. R., Espinoza, C. M., and Reisenegger, A., "Glitch time series and size distributions in eight prolific pulsars," Astron. Astrophys. **630**, A115 (2019).

[12] C. M. Espinoza, A. G. Lyne, B. W. Stappers, and M. Kramer, "A study of 315 glitches in the rotation of 102 pulsars," Mon. Not. R. Astron. Soc. **414**, 1679–1704 (2011).

[13] A Basu *et al.*, "The Jodrell bank glitch catalogue: 106 new rotational glitches in 70 pulsars," Mon. Not. R. Astron. Soc. **510**, 4049–4062 (2021).

[14] B. Shaw, A.G. Lyne, M.B. Mickaliger, *et al.*, "Jodrell Bank Pulsar Glitch Catalogue," `http://www.jb.man.ac.uk/pulsar/glitches.html` (2022), accessed 2022/10/11.

[15] G B Hobbs, R N Manchester, and L. Toomey, "The Australia Telescope National Facility Pulsar Catalogue: Glitch Parameters," `https://www.atnf.csiro.au/people/pulsar/psrcat/glitchTbl.html` (2022), accessed 2022/10/11.

[16] Joan Moragues, Luana M. Modafferi, Rodrigo Tenorio, and David Keitel, "Prospects for detecting transient quasi-monochromatic gravitational waves from glitching pulsars with current and future detectors," arXiv:2210.09907.

[17] Nils Andersson and Kostas D. Kokkotas, "Towards gravitational wave asteroseismology," Mon. Not. R. Astron. Soc. **299**, 1059–1068 (1998).

[18] Wynn C. G. Ho, D. I. Jones, Nils Andersson, and Cristóbal M. Espinoza, "Gravitational waves from transient neutron star f-mode oscillations," Phys. Rev. D **101**, 103009 (2020).

[19] Garvin Yim and D. I. Jones, "Gravitational waves from small spin-up and spin-down events of neutron stars," arXiv:2204.12869.

[20] J. Abadie *et al.* (LIGO Scientific Collaboration), "Search for gravitational waves associated with the August 2006 timing glitch of the Vela pulsar," Phys. Rev. D **83**, 042001 (2011).

[21] R. Abbott *et al.* (LIGO Scientific Collaboration, Virgo Collaboration and KAGRA Collaboration), "All-sky search for short gravitational-wave bursts in the third Advanced LIGO and Advanced Virgo run," Phys. Rev. D **104**, 122004 (2021).

[22] Jim Palfreyman, John M Dickey, Aidan Hotan, Simon Ellingsen, and Willem van Straten, "Alteration of the magnetosphere of the vela pulsar during a glitch," Nature **556**, 219—222 (2018).

[23] Gregory Ashton, Paul D. Lasky, Vanessa Graber, and Jim Palfreyman, "Rotational evolution of the Vela pulsar during the 2016 glitch," Nature Astronomy **3**, 1143–1148 (2019).

[24] `https://www.gw-openscience.org/detector_status/day/20161212/`.

[25] David Keitel *et al.*, "First search for long-duration transient gravitational waves after glitches in the vela and crab pulsars," Phys. Rev. D **100**, 064058 (2019).

[26] R. Abbott *et al.* (LIGO Scientific Collaboration, Virgo Collaboration and KAGRA Collaboration), "Narrow-band searches for continuous and long-duration transient gravitational waves from known pulsars in the LIGO-Virgo third observing run," Astrophys. J. **932**, 133 (2022).

[27] Luana M. Modafferi, Joan Moragues, and David Keitel (for the LIGO Scientific, Virgo and KAGRA collaborations), "Search for long-duration transient gravitational waves from glitching pulsars during LIGO—Virgo third observing run," J. Phys. Conf. Ser. **2156**, 012079 (2021).

[28] T Akutsu *et al.* (KAGRA Collaboration), "Overview of KAGRA: Detector design and construction history," Progress of Theoretical and Experimental Physics **2021** (2020).

[29] Bala R. Iyer *et al.*, *LIGO-India*, Tech. Rep. LIGO-M1100296 (IndIGO, 2011).

[30] James Clark, Ik Siong Heng, Matthew Pitkin, and Graham Woan, "Evidence-based search method for gravitational waves from neutron star ring-downs," Phys. Rev. D **76**, 043003 (2007).

[31] Brynmor Haskell and Andrew Melatos, "Models of Pulsar Glitches," Int. J. Mod. Phys. D **24**, 1530008 (2015).

[32] Elan Stopnitzky and Stefano Profumo, "Gravitational Waves from Gamma-Ray Pulsar Glitches," Astrophys. J. **787**, 114 (2014).

[33] T. Sidery, A. Passamonti, and N. Andersson, "The dy-

namics of pulsar glitches: contrasting phenomenology with numerical evolutions," Mon. Not. R. Astron. Soc. **405**, 1061–1074 (2010).
[34] R. Prix, S. Giampanis, and C. Messenger, "Search method for long-duration gravitational-wave transients from neutron stars," Phys. Rev. D **84**, 023007 (2011).
[35] T. G. Cowling, "The Non-radial Oscillations of Polytropic Stars," Mon. Not. R. Astron. Soc. **101**, 367–375 (1941).
[36] Kostas D. Kokkotas and Bernd G. Schmidt, "Quasinormal modes of stars and black holes," Living Rev. Relativity. **2**, 2 (1999).
[37] Nils Andersson and G. Comer, "Probing neutron-star superfluidity with gravitational-wave data," Phys. Rev. Lett. **87**, 241101 (2001).
[38] V. Ferrari, G. Miniutti, and J. A. Pons, "Gravitational waves from newly born, hot neutron stars," Mon. Not. R. Astron. Soc. **342**, 629–638 (2003).
[39] Dong Lai, "Secular instability of g-modes in rotating neutron stars," Mon. Not. R. Astron. Soc. **307**, 1001–1007 (1999).
[40] C. J. Krüger, W. C. G. Ho, and N. Andersson, "Seismology of adolescent neutron stars: Accounting for thermal effects and crust elasticity," Phys. Rev. D **92**, 063009 (2015).
[41] Ian Jones, *Calculating gravitational waveforms: examples*, Tech. Rep. LIGO-T1200476 (LIGO Laboratory, 2021).
[42] Kip S. Thorne, "Multipole expansions of gravitational radiation," Rev. Mod. Phys. **52**, 299–339 (1980).
[43] Nikolaos Stergioulas, "Rotating Stars in Relativity," Living Reviews in Relativity **6**, 3 (2003).
[44] Kostas D. Kokkotas and Nils Andersson, "Oscillation and instabilities of relativistic stars," in *14th SIGRAV Congress on General Relativity and Gravitation (SIGRAV 2000)* (2002) pp. 121–139.
[45] J. A. de Freitas Pacheco, "Do soft gamma repeaters emit gravitational waves?" Astron. Astrophys. **336**, 397–401 (1998).
[46] Erich Doneva, Daniela D. Gaertig, Kostas Kokkotas, and Christian Krüger, "Gravitational wave asteroseismology of fast rotating neutron stars with realistic equations of state," Phys. Rev. D **88**, 044052 (2013).
[47] `https://lscsoft.docs.ligo.org/lalsuite/lalsimulation/_l_a_l_sim_neutron_star_e_o_s_8c.html`.
[48] LIGO Scientific Collaboration, "LIGO Algorithm Library - LALSuite," free software (GPL) (2018).
[49] P. N. McDermott, H. M. van Horn, and J. F. Scholl, "Nonradial g-mode oscillations of warm neutron stars," Astrophys. J. **268**, 837–848 (1983).
[50] Andrew W. Steiner, James M. Lattimer, and Edward F. Brown, "The neutron star mass-radius relation and the equation of state of dense matter," Astrophys. J. **765**, L5 (2013).
[51] J. M. Lattimer, "Neutron Stars and the Nuclear Matter Equation of State," Annu. Rev. Nucl. Part. Sci. **71**, 433–464 (2021).
[52] Feryal Özel, Dimitrios Psaltis, Tolga Güver, Gordon Baym, Craig Heinke, and Sebastien Guillot, "The dense matter equation of state from neutron star radius and mass measurements," Astrophys. J. **820**, 28 (2016).
[53] A. Akmal, V. R. Pandharipande, and D. G. Ravenhall, "Equation of state of nucleon matter and neutron star structure," Phys. Rev. C **58**, 1804–1828 (1998).
[54] Benjamin D. Lackey, Mohit Nayyar, and Benjamin J. Owen, "Observational constraints on hyperons in neutron stars," Phys. Rev. D **73**, 024021 (2006).
[55] Sukrit Jaiswal and Debarati Chatterjee, "Constraining dense matter physics using f-mode oscillations in neutron stars," MDPI Physics **3**, 302–319 (2021).
[56] Marco Drago *et al.*, "coherent waveburst, a pipeline for unmodeled gravitational-wave data analysis," SoftwareX **14**, 100678 (2021).
[57] S. Klimenko, G. Vedovato, M. Drago, F. Salemi, V. Tiwari, G. A. Prodi, C. Lazzaro, K. Ackley, S. Tiwari, C. F. Da Silva, and G. Mitselmakher, "Method for detection and reconstruction of gravitational wave transients with networks of advanced detectors," Phys. Rev. D **93**, 042004 (2016).
[58] Sergey Klimenko *et al.*, "cwb pipeline library: 6.4.0," (2021).
[59] R. Abbott *et al.*, "Open data from the first and second observing runs of advanced ligo and advanced virgo," SoftwareX **13**, 100658 (2021).
[60] B. P. Abbott *et al.* (LIGO Scientific Collaboration, Virgo Collaboration and KAGRA Collaboration), "Prospects for observing and localizing gravitational-wave transients with advanced ligo, advanced virgo and kagra," Living Rev. Relativity. **23**, 3 (2020).
[61] B. P. Abbott *et al.* (LIGO Scientific Collaboration, Virgo Collaboration and KAGRA Collaboration), *Noise curves used for Simulations in the update of the Observing Scenarios Paper*, Tech. Rep. LIGO-T2000012 (LIGO Laboratory, 2022).
[62] M. Miyamoto and R. Nagai, "Three-dimensional models for the distribution of mass in galaxies." Publ. Astron. Soc. Jap. **27**, 533–543 (1975).
[63] D. A. Barros, J. R. D. Lépine, and W. S. Dias, "Models for the 3D axisymmetric gravitational potential of the Milky Way galaxy. A detailed modelling of the Galactic disk," Astron. Astrophys. **593**, A108 (2016).
[64] R. Dodson, D. Legge, J. E. Reynolds, and P. M. McCulloch, "The vela pulsar's proper motion and parallax derived from VLBI observations," Astrophys. J. **596**, 1137–1141 (2003).
[65] R. N. Manchester, G. B. Hobbs, A. Teoh, and M. Hobbs, "The Australia Telescope National Facility Pulsar Catalogue," Astron. J. **129**, 1993 (2005).
[66] P. B. Covas *et al.* (LSC Instrument Authors), "Identification and mitigation of narrow spectral artifacts that degrade searches for persistent gravitational waves in the first two observing runs of Advanced LIGO," Phys. Rev. D **97**, 082002 (2018).
[67] Derek Davis *et al.*, "LIGO detector characterization in the second and third observing runs," Classical and Quantum Gravity **38**, 135014 (2021).
[68] Reed Essick, Salvatore Vitale, Erik Katsavounidis, Gabriele Vedovato, and Sergey Klimenko, "Localization of short duration gravitational-wave transients with the early advanced LIGO and Virgo detectors," Astrophys. J. **800**, 81 (2015).
[69] Stephen Fairhurst, "Source localization with an advanced gravitational wave detector network," Class. Quant. Grav. **28**, 105021 (2011).
[70] Chris Pankow, Eve A. Chase, Scott Coughlin, Michael Zevin, and Vassiliki Kalogera, "Improvements in Gravitational-Wave Sky Localization with Expanded Networks of Interferometers," Astrophys. J. Lett. **854**,

L25 (2018).
[71] S. Klimenko, G. Vedovato, M. Drago, G. Mazzolo, G. Mitselmakher, C. Pankow, G. Prodi, V. Re, F. Salemi, and I. Yakushin, "Localization of gravitational wave sources with networks of advanced detectors," Phys. Rev. D **83**, 102001 (2011).
[72] M. Yu *et al.*, "Detection of 107 glitches in 36 southern pulsars," Mon. Not. R. Astron. Soc. **429**, 688–724 (2013).
[73] G. Ashton, R. Prix, and D. I. Jones, "Statistical characterization of pulsar glitches and their potential impact on searches for continuous gravitational waves," Phys. Rev. D **96**, 063004 (2017).
[74] Swetha Arumugam and Shantanu Desai, "Classification of Pulsar Glitch Amplitudes using Extreme Deconvolution," arXiv:2206.02751.
[75] J. Richard Shaw, Kris Sigurdson, Ue-Li Pen, Albert Stebbins, and Michael Sitwell, "All-Sky Interferometry with Spherical Harmonic Transit Telescopes," Astrophys. J. **781**, 57 (2014).
[76] A. Weltman *et al.*, "Fundamental physics with the Square Kilometre Array," Publ. Astron. Soc. Austral. **37**, e002 (2020).
[77] ET Science Team, "Einstein gravitational wave Telescope conceptual design study," (2011), eT-0106C-10.
[78] Matthew Evans *et al.*, "A Horizon Study for Cosmic Explorer: Science, Observatories, and Community," arXiv:2109.09882.
[79] K. Ackley *et al.*, "Neutron Star Extreme Matter Observatory: A kilohertz-band gravitational-wave detector in the global network," Publ. Astron. Soc. Austral. **37**, e047 (2020).
[80] Burkhard Zink, Oleg Korobkin, Erik Schnetter, and Nikolaos Stergioulas, "Frequency band of the f-mode chandrasekhar-friedman-schutz instability," Phys. Rev. D **81**, 084055 (2010).
[81] Georgios Lioutas and Nikolaos Stergioulas, "Universal and approximate relations for the gravitational-wave damping timescale of f-modes in neutron stars," Gen. Rel. Grav. **50**, 12 (2018).
[82] P. N. McDermott, H. M. van Horn, and J. F. Scholl, "Nonradial g-mode oscillations of warm neutron stars," Astrophys. J. **268**, 837–848 (1983).
[83] Lee Lindblom and Randall J. Splinter, "The Accuracy of the Relativistic Cowling Approximation," Astrophys. J. **348**, 198 (1990).
[84] Shijun Yoshida and Yasufumi Kojima, "Accuracy of the relativistic Cowling approximation in slowly rotating stars," Mon. Not. R. Astron. Soc. **289**, 117–122 (1997).
[85] Subrahmanyan Chandrasekhar and V. Ferrari, "On the non-radial oscillations of a star," Proc. Roy. Soc. Lond. A **432**, 247–279 (1991).
[86] Subrahmanyan Chandrasekhar, Valeria Ferrari, and Roland Winston, "On the Non-Radial Oscillations of a Star II. Further Amplifications," Proc. Roy. Soc. Lond. A **434**, 635–641 (1991).
[87] Omar Benhar, Valeria Ferrari, and Leonardo Gualtieri, "Gravitational wave asteroseismology reexamined," Phys. Rev. D **70**, 124015 (2004).
[88] Cecilia Chirenti, Gibran H. de Souza, and Wolfgang Kastaun, "Fundamental oscillation modes of neutron stars: Validity of universal relations," Phys. Rev. D **91**, 044034 (2015).
[89] Bikram Keshari Pradhan and Debarati Chatterjee, "Effect of hyperons on f-mode oscillations in neutron stars," Phys. Rev. C **103**, 035810 (2021).
[90] Bikram Keshari Pradhan, Debarati Chatterjee, Michael Lanoye, and Prashanth Jaikumar, "General relativistic treatment of f-mode oscillations of hyperonic stars," Phys. Rev. C **106**, 015805 (2022).
[91] H. C. Das, Ankit Kumar, S. K. Biswal, and S. K. Patra, "Impacts of dark matter on the f-mode oscillation of hyperon star," Phys. Rev. D **104**, 123006 (2021).
[92] Xueling Mu, Bin Hong, Xia Zhou, Guansheng He, and Zhongwen Feng, "The influence of entropy and neutrinos on the properties of protoneutron stars," The European Physical Journal A **58** (2022), 10.1140/epja/s10050-022-00721-x.